



**HAL**  
open science

## Nuclear magnetic relaxation dispersion investigations of water retention mechanism by cellulose ethers in mortars

Laetitia Patural, Jean-Pierre Korb, Alexandre Govin, Philippe Grosseau,  
Bertrand Ruot, Olivier Devès

### ► To cite this version:

Laetitia Patural, Jean-Pierre Korb, Alexandre Govin, Philippe Grosseau, Bertrand Ruot, et al.. Nuclear magnetic relaxation dispersion investigations of water retention mechanism by cellulose ethers in mortars. Cement and Concrete Research, 2012, 42 (10), pp.1371-1378. 10.1016/j.cemconres.2012.06.002 . hal-00762106

**HAL Id: hal-00762106**

**<https://hal.science/hal-00762106>**

Submitted on 30 Jan 2013

**HAL** is a multi-disciplinary open access archive for the deposit and dissemination of scientific research documents, whether they are published or not. The documents may come from teaching and research institutions in France or abroad, or from public or private research centers.

L'archive ouverte pluridisciplinaire **HAL**, est destinée au dépôt et à la diffusion de documents scientifiques de niveau recherche, publiés ou non, émanant des établissements d'enseignement et de recherche français ou étrangers, des laboratoires publics ou privés.

1                   **Nuclear magnetic relaxation dispersion investigations**  
2                   **of water retention mechanism by cellulose ethers in mortars**

3  
4   **LAETITIA PATURAL<sup>(1)</sup>, JEAN-PIERRE KORB<sup>(2)\*</sup>, ALEXANDRE GOVIN<sup>(1)</sup>, PHILIPPE**  
5   **GROSSEAU<sup>(1)</sup>, BERTRAND RUOT<sup>(3)</sup>, OLIVIER DEVÈS<sup>(3)</sup>**

6  
7   <sup>(1)</sup> *École Nationale Supérieure des Mines de Saint-Étienne ; Centre SPIN, LPMG FRE 3312*  
8    *158 Cours Fauriel, 42023 Saint-Étienne Cedex 2, France*

9   <sup>(2)</sup> *Physique de la Matière Condensée, Ecole Polytechnique-CNRS, Route de Saclay,*  
10   *91128 Palaiseau Cedex, France*

11   <sup>(3)</sup> *Université Paris-Est, Centre Scientifique et Technique du Bâtiment ; Département*  
12    *Enveloppe et Revêtements / Division Enduits, Mortiers et Colles, 84 avenue Jean Jaurès,*  
13    *77447 Marne-la-Vallée Cedex 2, France*

14  
15  
16  
17  
18  
19  
20   \* Corresponding author:     jean-pierre.korb@polytechnique.fr

21

22 **ABSTRACT**

23

24 We show how nuclear magnetic spin-lattice relaxation dispersion of protons-water  
25 (NMRD) can be used to elucidate the effect of cellulose ethers on water retention and  
26 hydration delay of freshly-mixed white cement pastes. NMRD is useful to determine the  
27 surface diffusion coefficient of water, the specific area and the hydration kinetics of the  
28 cement-based material. In spite of modifications of the solution's viscosity, we show that the  
29 cellulosic derivatives do not modify the surface diffusion coefficient of water. Thus, the  
30 mobility of water present inside the medium is not affected by the presence of polymer.  
31 However, these admixtures modify significantly the surface fraction of mobile water  
32 molecules transiently present at solid surfaces. This quantity measured, for the first time, for  
33 all admixed cement pastes is thus relevant to explain the water retention mechanism.

34

35

36

37

38 **KEYWORDS:** *cellulose ether, cement paste, NMR relaxometry, surface diffusion coefficient,*  
39 *water retention.*

40

41

## 42 1. Introduction

43 Cellulose ethers (*CE*) are well known water-soluble semi-synthetic polymers derived from  
44 cellulose, the most abundant polysaccharide in nature. This polymer is build up from 1,4-  
45 anhydroglucose units linked through  $\beta$ -1,4 glycoside bonds. Among the various derivatives of  
46 this polymer, hydroxypropyl methyl cellulose (HPMC, Fig. 1a), hydroxyethyl methyl  
47 cellulose (HEMC, Fig. 1b) and hydroxyethyl cellulose (HEC, Fig. 1c) are extensively used in  
48 the formulation of various industrial products encountered in food stuffs, pharmaceuticals and  
49 building materials. For instance, the presence of cellulose ethers (*CE*) in mortars enhances  
50 drastically the water-retention [1]. Some experimental devices have been designed to  
51 evidence such water retention **on a macroscopic lengthscale** (Fig. 2). This specific property of  
52 *CE* is crucial to achieve sufficient mortar-substrate adhesion **when the mortar is applied in**  
53 **thin layers on highly absorbent substrates**. Other properties are also affected by *CE*, such as  
54 the delay of hydration and setting [2-3]. Some HPMC, HEMC and HEC were characterized in  
55 terms of their effect on mortar water retention [4-5]. A few recent works have been concerned  
56 with the remarkable mechanism of water retention capacity. A significant influence of the  
57 polymer molecular parameters like molecular weight and substitution degrees was evidenced  
58 [5], but no clear water retention mechanism could be clearly identified. During evaporation,  
59 no admixture loss is occurring, due to the very low vapour pressure of this admixture and a  
60 decrease in the water chemical potential occurs [6]. A decrease of water mobility due to the  
61 jamming of the diffusion space by the polymer molecules is even expected [7, 8]. However, a  
62 recent pulsed gradient field NMR study proved that the macroscopic bulk water self diffusion  
63 coefficient is not modified in *CE* solution or in admixed cement pastes [9]. Moreover, the  
64 interdiffusion imaging experiments demonstrated also that the water diffusion at the paste  
65 interface is not affected by the presence of cellulosic admixture [9]. So, the possibility of a  
66 potential microscopic diffusion barrier specifically at the cement hydrates interfaces is still

67 controversial and the origin of the mechanism of water retention due to *CE* admixture is still  
68 an open question.

69 The aim of the present work is precisely to answer the latter question and to propose a  
70 realistic mechanism for the water retention in presence of *CE* in mortars. To limit the  
71 interaction between mineral components, the system was reduced to a white cement paste. We  
72 propose another NMR measurement to sense the proton species dynamics specifically at the  
73 solid interface. Our primary measurement here is the magnetic field dependence or relaxation  
74 dispersion of the proton spin-lattice relaxation rate constant  $1/T_1$  (NMRD, [10, 11]) in neat  
75 (without *CE*) and *CE*-admixed white cement pastes. For cement pastes, the NMRD technique  
76 is neither invasive nor destructive because one measures only the proton NMR response  
77 coming from the mixing water itself. This technique has proven useful to give a direct reliable  
78 value of the specific surface area of a cement-based material [12]. The remarkable features of  
79 the relaxation dispersion support an interpretation in terms of coupled solid/liquid relaxation  
80 at pore interfaces, surface diffusion and nuclear paramagnetic relaxation. The measurement is  
81 sufficiently fast to be applied continuously during the progressive hydration and setting of the  
82 material. In this study, we show the time evolution of the NMR-based specific surface area  
83 and the amount of water transiently present at the solid and growing interface. We also  
84 discuss the effects of the different *CE* and Starch Ether (*SE*) used on the surface diffusion  
85 coefficient and on the relative amount of water transiently present at the solid and growing  
86 interface.

## 87 2. Experiments

### 88 2.1. Mineral and organic products

89 Cement pastes were prepared with white cement in order to facilitate NMR relaxation  
90 experiments. However, we showed before by electronic spin resonance (ESR) that

91 paramagnetic  $Fe^{3+}$  ions were clearly present in white cement (see Fig. 6 in ref. [12]). The  
92 amount of such paramagnetic ferric ions was quantitatively evaluated through a double  
93 integration of this calibrated ESR spectrum [12]. Chemical analysis of this cement was  
94 performed by X-ray fluorescence spectroscopy (XRF). The phase compositions were  
95 calculated using Bogue's formula with a correction on CaO due to sulfates [13]. The cement  
96 composition is given in **Table 1**.

97 The admixtures used are cellulose ethers (*CE*) of chemical structures given in Fig. 1. The  
98 admixture amount was equal to 0.27% (compared to cement). The characteristics of the main  
99 physical-chemistry properties and labels used for the cellulose ethers studied are summarized  
100 in **Table 2**. The number of substituted hydroxyl groups per anhydroglucose unit is expressed  
101 as degree of substitution (*DS*). Moreover the molar ratio of alkoxy groups in the side chains to  
102 cellulose is expressed as the average molecular substitution (*MS*) [14]. The cellulose ether  
103 weight-average molecular mass ( $\bar{M}_w$ ) was determined using size exclusion chromatography  
104 [5, 15]. We have prepared different samples with increased molecular mass  $\bar{M}_w =$   
105 {225, 630, 910} *kDa* labeled J1, J2 and J3, respectively (**Table 2**). Others starch ethers were  
106 also investigated, those are polymers providing very different water retentions (**Table 3**).

## 107 2.2. Water retention

108 For water retention measurements, mortars were prepared according to the CEReM  
109 mixture proportions consisting in 65% sand, 30% ordinary Portland cement (CEM I 52.5 R),  
110 5% calcareous filler with a water to cement ratio  $w/c=1$  [16]. Mixing procedure was in  
111 accordance with EN 196-1 [17]. Admixture amount (0.27%) was in addition to the total dry  
112 mixture (*i.e.* cement, sand and filler). The water retention capacity was assessed using the test  
113 from an American standard (ASTM C1506-09), based on application of an air depression  
114 [18]. It is also used in France for assessing one-coat renderings [19].

115 The experimental device to measure water retention is shown in Fig. 2. It is composed  
116 of a perforated dish attached to a vacuum assembly by a funnel. The dish was filled in with  
117 the freshly mixed mortar and the vacuum was adjusted to maintain a depression of 50 mm Hg  
118 for 15 min. The initial weight of mixing water is labeled as  $W_0$ . Its loss ( $W_1$ ) is weighted after  
119 the depression period. Hence, the water retention  $WR$  was defined by the following equation:

$$120 \quad WR (\%) = \frac{W_0 - W_1}{W_0} \times 100 \quad (1)$$

121

### 122 2.3. Experiments of proton nuclear magnetic relaxation dispersion (NMRD) in admixed 123 cement pastes

124 We performed proton nuclear magnetic relaxation dispersion (NMRD) on a fast-field  
125 cycling spectrometer from *Stelar s.r.l., Mede, Italy*, where the polarization magnetic field is  
126 0.5 T while the evolution magnetic field ranges from 0.25 mT to 0.5 T. All samples were  
127 introduced into a 7 mm-tube which was inserted into a 10 mm-diameter standard NMR tube.  
128 Cement pastes were prepared with a water/cement ratio  $w/c=0.4$  in order to have an  
129 appropriate consistency and for facilitating the NMR measurements at low fields. The proton  
130 nuclear magnetization originally at thermal equilibrium is oriented toward the external steady  
131 polarized magnetic field (typically 0.5 T). The external field is instantaneously decreased (in  
132 about 3ms) at an evolution magnetic field chosen in the range from 0.25 mT to 0.5 T in which  
133 the magnetization relaxes, then the magnetic field is fixed to 0.25T in which a classical **free**  
134 **induced longitudinal magnetization decay measurement is then** achieved by applying a  $\pi/2$   
135 pulse. **Such a fast field cycling sequence is very well documented [10, 11].** The temperature  
136 was fixed at 298K. The experiment was repeated over a large range of proton Larmor  
137 frequencies  $\omega/2\pi$  (10 kHz - 20 MHz) in order to obtain the complete dispersion profile of the  
138 longitudinal spin-lattice relaxation rate  $R_1(\omega)=1/T_1(\omega)$ .

139 Basically, proton NMR relaxation is a stimulated (non spontaneous) phenomenon driven  
140 by the coupling of the proton spins to the magnetic noise induced by molecular motions  
141 (translation, rotation, exchange, etc). Varying the magnetic field changes the proton Larmor  
142 frequency  $\omega_l/2\pi$ , and thus allows exploring the time scales of the magnetic fluctuations  
143 (noise) to which the nuclear spin relaxation is sensitive. For diffusive liquids, NMRD gives  
144 also a rich source of dynamical information over a large range of length scales, from localized  
145 and fast motions at large frequency to a delocalized and slow motions at low frequency.

146 We propose two kinds of NMRD experiments for white admixed cement pastes. The first  
147 experiment consists of measuring the magnetic field dependence of the proton spin-lattice  
148 relaxation rate  $R_1(\omega_l) = 1/T_1(\omega_l)$  of various admixtures of different CE (Figs. 3, 4). The  
149 second experiment consists in probing continuously the spin-lattice relaxation rate  $1/T_1$   
150 ( $\omega_l=2\pi \times 10\text{kHz}$ ,  $t_{hydr}$ ) at a fixed and low frequency (10kHz) during the inducing period of  
151 cement paste with various admixtures of different CE (Figs. 5, 7- 9). During this period, we  
152 observe a monoexponential longitudinal magnetization decay that rules out any distribution of  
153  $T_1$ , the non exponential relaxation only appearing after ten hours of hydration [see Fig. 7 of  
154 12]. The continuous measurement of  $1/T_1(\omega_l=2\pi \times 10\text{kHz}, t_{hydr})$  in presence of various  
155 admixtures of cellulose ethers allows us to monitor the evolution of the specific surface area  
156  $S(t_{hydr})/V$ , of the material during the hydration.

### 157 3. Theory of nuclear magnetic relaxation dispersion (NMRD) in cement pastes

158 We proposed previously a theoretical model necessary for interpreting all the NMRD  
159 relaxation features reported in Figs. 3 and 4 [12, 20-22]. In the following, we just present a  
160 self-contained outline of the basic hypothesis and equations of the model needed for probing  
161 the specific surface area and the water surface diffusion coefficient at the growing interface of  
162 the adjuvanted cement paste.



163 (i) Basically, when considering the nuclear relaxation of water embedded in solid hydrated  
 164 cement, there are coupled relaxation equations for the solid and liquid magnetizations at  
 165 pore interfaces. The return to equilibrium of either solid or liquid proton spin  
 166 magnetization is thus a bilinear combination of exponentials with the rate constants for  
 167 slow ( $R_{slow}$ ) and fast ( $R_{fast}$ ) components [23, 24] given by:

$$168 \quad R_{slow} = \frac{1}{2} \left\{ R_{1,s} + R_{1,w} + k(1+1/F) \mp \left[ \left[ R_{1,s} - R_{1,w} - k(1-1/F) \right]^2 + 4k^2/F \right]^{1/2} \right\} \quad (2)$$

169 Here  $R_{1,s}=1/T_{1,s}$  and  $R_{1,w}(\omega_l)$  are the spin-lattice relaxation rate constants associated to  
 170 solid protons and confined liquid proton-water, respectively.  $k$  is the dipolar cross-  
 171 relaxation rate from the water protons to the solid proton species and  $F$  is the ratio of the  
 172 solid-proton magnetization to the liquid-proton population at equilibrium:  $F = m_s^{eq} / m_w^{eq}$ .

173 (ii) In most applications of field cycling experiments, the rapidly decaying component  $R_{fast}$  of  
 174 the bi-exponential decay is not detected because of instrumental limitations and the  
 175 slowly decaying component  $R_{slow}$  dominates the observations. Moreover, for the confined  
 176 liquid, the intermolecular dipole-dipole interaction couples the water spin relaxation to  
 177 that of the solid and the magnetic field dependence of the immobilized solid spin system.

178 (iii) The molecular exchange between the solid and liquid phases is sufficiently fast compared  
 179 to their respective individual proton relaxation times that a single  $R_{1,w}(\omega_l)$  exists given by  
 180 a linear combination of a bulk and a surface contributions [25]. The latter is weighted by  
 181 the surface to volume ratio  $S/V$  present at a given time of hydration at the solid/liquid  
 182 interface [20].

183 (iv) The spin-lattice relaxation rate  $R_{1,w}(\omega_l)$  for the confined proton-liquid has a bilogarithmic  
 184 frequency dependence [26] that comes unambiguously from the two dimensional  
 185 diffusion of the water molecules along the pore surface modulating the dipole-dipole  
 186 interaction between the proton species and the paramagnetic  $Fe^{3+}$  ions fixed at the surface

187 [12, 20-22]. On the contrary, in the frequency range studied, the spin-lattice relaxation  
 188 rate for the solid protons  $R_{I,s}$  does not depend on the frequency [20] and the bulk  
 189 relaxation rate  $R_{I,bulk}$  is frequency independent [27].

190 (v) At high frequencies (10-100 MHz), the nuclear paramagnetic relaxation controls the  
 191 proton relaxation [28]. This gives a typical bump in the NMRD profiles in this frequency  
 192 range [29] that is not seen here.

193 (vi) The conservation of these frequency dependencies during the progressive hydration and  
 194 the evolution of  $1/T_1(\omega_I, t_{hydr})$  with the hydration time allowed us to renormalize the  
 195 NMRD data to a single master curve  $1/T_1(\omega_I, t_{hydr}) \propto [S_{p,NMR}(t_{hydr})]f(\omega_I)$  [20],  
 196 where  $S_{p,NMR}$  is a NMR-based specific surface area of the hydrated cement that appears to  
 197 be directly proportional to the degree of advancement of chemical reaction [20].

198 Taking these considerations into account, we find that the following theoretical analytical  
 199 expression of  $R_{I,w}$  allows us to reproduce all the observed frequency features:

200

$$\begin{aligned}
 R_{I,w}(\omega_I > \omega_d) = & R_{I,bulk} + \frac{x\mathcal{E}}{60} \sigma_S \rho_w S_{p,NMR} (\gamma_I \gamma_S \hbar)^2 S(S+1) \times \\
 & \left[ \frac{\pi}{\mathcal{E}^4} \tau_m \left[ 3 \ln \left( \frac{1 + \omega_I^2 \tau_m^2}{(\tau_m/\tau_s)^2 + \omega_I^2 \tau_m^2} \right) + 7 \ln \left( \frac{1 + \omega_S^2 \tau_m^2}{(\tau_m/\tau_s)^2 + \omega_S^2 \tau_m^2} \right) \right] \right. \\
 & \left. + \frac{8n\mathcal{E}^2}{r_{IS}^6} \tau_c \left[ \frac{7}{1 + \omega_S^2 \tau_c^2} + \frac{3}{1 + \omega_I^2 \tau_c^2} \right] \right] \quad (3)
 \end{aligned}$$

202

203 where  $\rho_w$  is the density of the water,  $\mathcal{E} = 3.0 \text{ \AA}$  is the water molecule size,  $x\mathcal{E} \sim 10 \text{ \AA}$  is an  
 204 interfacial water layer according to previous calorimetry studies [30] and  $r_{IS} = 2.7 \text{ \AA}$  is the  
 205 distance of minimal approach between  $I$  and  $S$  spins. The electronic spin  $S = 5/2$  for  $Fe^{3+}$ ;  $n \approx$   
 206  $I$  is the number of bounded water molecules in the ligand field of the  $Fe^{3+}$  ions. Since the  
 207 gyromagnetic ratio of the electron,  $\gamma_S$ , is much larger than that of the proton,  $\gamma_I$  ( $\gamma_S = 658.21$

208  $\gamma$ ), the electronic frequency is  $\omega_S = 658.21 \omega$ . In Eq. 3,  $N_S/N = x\varepsilon\rho_w S_{p,NMR}$  represents the ratio  
 209 of the number of water molecules transiently present at the pore surface,  $N_S$ , to the total  
 210 number,  $N$ , of exchangeable water molecules in the sample. Also in Eq. (3),  $\tau_m$  is the  
 211 correlation time characterizing the two-dimensional diffusion of the proton species at the  
 212 surface of the pores. We introduce also the effects of the finite time of residence  $\tau_S \gg \tau_m$  for  
 213 the mobile proton species at the surface of the pores by an exponential cut-off in the time  
 214 dependence of the pair correlations  $IS$ . The correlation time  $\tau_c$  of the nuclear paramagnetic  
 215 relaxation is given by  $1/\tau_c = 1/\tau_{ex} + 1/T_{1Fe} \approx 1/T_{1Fe}$  where  $\tau_{ex}$  ( $\tau_{ex} \gg T_{1Fe}$ ) is the lifetime of water  
 216 in the ligand field of the ferric ions. The electronic spin-lattice relaxation time of the  
 217 paramagnetic impurity  $T_{1Fe}$  (of the order of  $2 \cdot 10^{-11}$ s) is constant at low frequency and has a  
 218 frequency dependence at higher frequency defined in ref [12, 20, 28]. The relaxation rate in  
 219 the bulk phase,  $R_{Ibulk} \sim 0.3 \text{ s}^{-1}$  is caused by the fast molecular reorientations and translations  
 220 and is independent of frequency in the low field range studied [27]. Last, Substituting Eq. (3)  
 221 into Eq. (2) gives the theoretical expression that we can compare with the experiments in Figs.  
 222 3 and 4.

## 223 4. Results and discussion

### 224 4.1. Water retention of freshly-mixed mortars

225 The water retention capacity of each admixed mortar was evaluated; the results are  
 226 presented in **Table 2 and 3**. The cellulose ethers improved water retention up to 98.9% for  
 227 HPMC J3. With respect to the water retention capacity of the non-admixed mortar (64.5%),  
 228 this represents a very large increase. However the starch ethers procure very different water  
 229 retention capacities ranging from 66.2% to 92.6%.

#### 230 4.2. Surface diffusion coefficient

231 The surface diffusion coefficient is obtained from a fitting procedure with Eqs. (2) and (3)  
232 on the NMRD profiles of Figs. 3 and 4. Fig. 3a shows the NMRD profiles for the neat  
233 (without CE) white cement paste. Fig. 3b shows the NMRD profiles of a white cement paste  
234 admixed with HPMC J3. On both cases, we have varied the duration of the experiments by  
235 changing the number of frequencies explored. Using thirty points takes some time (about 5  
236 minutes per point) and we note that frequency profiles were affected by the kinetics of cement  
237 hydration. Indeed, the time needed to register one complete profile is about 2h30. In  
238 consequence, we could not observe the characteristic 10/3 slope ratio of the bilogarithmic  
239 frequency dependence usually found in cement based materials [20]. A simple procedure that  
240 allows limiting such a kinetic effect during the measurements is to decrease the number of  
241 frequency points on the profiles. One observes on Figs. 3a, b that reducing the experimental  
242 time to 45 minutes allows decreasing the kinetic effect. For instance, we observe that the first  
243 12 points almost merge at high frequency, then, the gap between the two profiles increases  
244 with time. In consequence, all NMRD dispersion curves of this work were obtained with  
245 twelve different and logarithmically spaced frequency values between 0.01 and 15 MHz to  
246 avoid the problems due to kinetics of cement hydration. This procedure allows a quite  
247 reasonable fit of the plateau dependence at low frequency and the bilogarithmic dependence at  
248 higher frequency (Figs. 3 and 4).

249 Fig. 4a presents the proton NMRD data obtained for different admixed cement pastes with  
250 three HPMC (J1, J2 and J3). The correlation time  $\tau_m$  is determined using the model described  
251 above. For these four different cement pastes, we find similar results for the translational  
252 surface diffusion approximately equal to  $\tau_m \approx 1ns$  and  $\tau_s \approx 10 \mu s$ . This suggests a pore scale  
253 invariance of water dynamics at the pore surface in C-S-H whatever the paste composition.  
254 This value of  $\tau_m$  is in agreement with previous studies performed on cement pastes or on

255 mortars [20, 21]. The translational diffusion coefficient  $D_{surf}$  at the pore surface can be  
256 deduced from the Stokes-Einstein relationship:  $D_{surf} = \varepsilon^2 / (4\tau_m)$  where  $\varepsilon = 3\text{\AA}$  is the water  
257 molecules size. For all cement pastes (admixed or not), the surface diffusion coefficient is  
258 about  $D = 2.25 \cdot 10^{-11} \text{m}^2 \cdot \text{s}^{-1}$  *i.e.* about 1/100 of that of bulk water at 23°C. In consequence,  
259 the presence of cellulose ethers in cement paste does not modify the surface diffusion  
260 coefficient at the pore surface. This result is similar to those obtained in the macroscopic scale  
261 by pulsed field gradient NMR showing that the CE does not modify the diffusion coefficient  
262 of water in the bulk [9].

263 The effect of starch ethers was also investigated with M1 and M4. These polymers provide  
264 very different water retentions (92.6% and 66.2% respectively). The protocol was identical to  
265 that of cement pastes containing cellulose ethers. The results are shown on Fig. 4b. The  
266 translational correlation times are also  $\tau_m \approx 1 \text{ns}$  and  $\tau_s \approx 10 \mu\text{s}$  for the admixed cement paste  
267 with M1 and M4 respectively. This demonstrates that the translational diffusion coefficient at  
268 the surface of the solid interfaces is not affected by starch ether's presence.

269 These experiments thus demonstrate that cellulose and starch derivatives do not change the  
270 surface diffusion coefficient of water. The water mobility at pore surface is thus not modified  
271 in presence of such polymers.

#### 272 4.3. Specific surface area and relative quantity of water transiently present at pore surface

273 On Figs. 3 and 4, one observes a constant value for  $1/T_1$  when the proton frequency  
274 becomes  $\omega_l < \omega_d = 2\pi \times 30 \text{ kHz}$ . Such a cross-over frequency  $\omega_d$  is of the order of the dipolar  
275 interaction in the solid state between two protons separated by 0.155 nm. On this low  
276 frequency range, the confined proton liquid explores relaxation processes induced by  
277 characterized long correlation times encountered in the solid state:  $\tau_{rigid} = 1/\omega_d = 5.3 \mu\text{s}$ . We  
278 have shown in Section 3 (i) that owing to the cross relaxation process, the intermolecular  
279 dipole-dipole interaction then couples the water spin relaxation to that of the solid and the

280 magnetic field dependence of the immobilized spin system. From a mathematical point of  
 281 view, Eq. (2) tends to the constant relaxation rate of the solid matrix  $R_{I_s}$  when the dipolar  
 282 cross-relaxation rate is lower than the individual relaxation  
 283 rates, *i. e.*:  $k \ll R_{1,w}, R_{1,s}$  and  $|R_{1,w} - R_{1,s}|$  and providing that  $F \ll 1$  and  $k/F > k$ :

284

$$285 \quad R_{slow}(\omega_I < \omega_d) \approx R_{1,s} + k/F, \text{ with } R_{1,s} \equiv R_{1,w}(\omega_I = \omega_d) = Cte \quad (4)$$

286

287 The observed data presented in Fig. 5 confirm the plateau observed at low frequency (at 10  
 288 kHz) for  $R_{slow}$  during the first hundred minutes. Then, relaxation rate increases due to cement  
 289 hydration and development of the specific surface area. Moreover, a zoom on the Fig. 5  
 290 shows that small but significant differences exist between each adjuvanted cement pastes.  
 291 The observed plateau for frequency below  $\omega_d$  is thus characteristic of the rigid-lattice limit of  
 292 the solid-proton hydrates. The absolute value of such a plateau, measured for instance at 10  
 293 kHz, is thus indicative of the specific surface area precisely at the solid-liquid interface:

$$294 \quad R_{slow}(\omega_I = 2\pi \times 10kHz, t_{hydr}) \approx R_{1,s}(t_{hydr}) \approx R_{1,w}(\omega_I = \omega_d, t_{hydr}) \quad (5)$$

295 As the correlation times  $\tau_m$  and  $\tau_s$  are constants whatever the cement paste composition, the  
 296 continuous measurement of  $R_{slow}(t_{hydr})$  at a fixed and low frequency  $\omega_I = 2\pi \times 10kHz$ , allows  
 297 to probe directly the time evolution of the specific surface area of the cement paste  $S_{p,NMR}$ :

298

$$299 \quad S_{p,NMR}(t_{hydr}) = \frac{1/T_{1,observed}(10kHz, t_{hydr})}{\frac{x\epsilon\pi}{60\epsilon^4} \sigma_S \rho_w (\gamma_I \gamma_S \hbar)^2 S(S+1)\tau_m \left[ 3 \ln \left( \frac{1 + \omega_d^2 \tau_m^2}{(\tau_m/\tau_s)^2 + \omega_d^2 \tau_m^2} \right) + 7 \ln \left( \frac{1 + 659^2 \omega_d^2 \tau_m^2}{(\tau_m/\tau_s)^2 + 659^2 \omega_S^2 \tau_m^2} \right) \right]}$$

300

(6)

301 The continuous measurement of  $1/T_1(\omega_f=2\pi\times 10\text{kHz}, t_{hydr})$  in presence of various  
302 admixtures of cellulose ethers thus allows to monitor the evolution of the specific surface area  
303  $S_{P,NMR}(t_{hydr})$ , of the material during the hydration.

304

#### 305 4.4. How NMR relaxation can elucidate water retention mechanisms

306

307 In the very early aged of the hydration, the amount of CSH is not very large and the  
308 admixed polymer is still in the interstitial solution within the pores of the paste, even if the  
309 cellulose ethers are rather large. The relaxation of the mobile proton-water thus will be  
310 influenced by the presence of the polymer. We show that measuring the time evolution of the  
311 spin-lattice relaxation rate  $R_{slow}(10\text{ kHz}, t_{hydr})$  at 10 kHz, especially in the first minutes of  
312 hydration allows probing quantitatively the relative population of water transiently present at  
313 the solid hydrate surfaces  $N_S/N(t_{hydr})$ .

314 On Fig. 5, the continuous lines exhibit the time evolution of  $R_{slow}(10\text{ kHz}, t_{hydr})$  for the non  
315 adjuvanted (neat) white cement and with HPMC J1, J2, J3 admixtures. The periods  $d_{CE}$   
316 during which the plateau remains constant are evidenced ( $d_0$  is related to neat cement) and  
317 ordered as followed:

$$318 \quad d_0 = 11\text{ min} < d_{J3} = 60\text{ min} < d_{J2} = 79\text{ min} < d_{J1} = 107\text{ min}.$$

319 This period  $d_{CE}$ , measured at low frequency, is a clear indicator of the delay of hydration  
320 induced by the CE polymer introduced into the material. The fact that  $d_0$  stays much smaller  
321 than the other  $d_{CE}$  is a clear indication of the delayed hydration and setting induced by the  
322 HPMC J1, J2, J3 admixtures. We show on Fig. 6, that one can correlate these delays of  
323 hydration measured by NMRD to the ones measured from isotherm calorimetry  
324 measurements (determined using the method described in ref. [31]) on similar materials. The  
325 quasi linear dependence ( $r^2=0.99$ ) shows very good accuracy between the microscopic  
326 (NMRD) and macroscopic (calorimetry) measurements.

327 Another important parameter can be extracted from the behaviour of the time evolution of  
 328  $R_{slow}(10\text{ kHz}, t_{hydr})$  during the first 100 minutes of hydration. This is the value of the plateau  
 329 itself, noted,  $R_{CE} = R_{slow,observed}(10\text{kHz}, t_{hydr})$  which depends critically on the nature of the  
 330 admixtures. The results found for the neat white cement paste and HPMC-admixed cement  
 331 pastes J1, J2, J3 are ordered as followed:

$$R_0 = 30\text{ s}^{-1} < R_{J1} = 35,9\text{ s}^{-1} < R_{J2} = 36,3\text{ s}^{-1} < R_{J3} = 37,6\text{ s}^{-1}$$

332 where  $R_0$  is the value of the low-frequency plateau for neat cement. According to Eqs. (2) and  
 333 (3),  $R_{CE}$  is proportional to the correlation time  $\tau_m$  and directly related to the relative amount  
 334 of water  $N_S/N$  transiently present during the first 100 minutes at proximity of solid interfaces  
 335 that is proportional to the specific surface area:

$$336 \frac{N_S(t_{hydr} < d_{CE})}{N} = x\varepsilon\rho_w S_{p,NMR}(t_{hydr} < d_{CE}) \quad (7)$$

337  
 338 where  $S_{p,NMR}(t_{hydr})$  is defined in Eq. (6). Substitution of all the parameters measured or defined  
 339 above in Eq. (7) and owing to the observation that  $\tau_m \approx 1\text{ ns}$  and  $\tau_s \approx 10\ \mu\text{s}$  are universal for all  
 340 the cement-based materials, one obtains a proportion  $N_S(t_{hydr}=2\text{ min})/N = 1.06\%$  for the neat  
 341 white cement paste and  $N_S(t_{hydr}=2\text{ min})/N = 1.36\%$  for the admixed cement pastes with  
 342 HPMC J3. One obtains intermediate values for the other admixtures HPMC J1 and HPMC J2.  
 343 The fact to probe, in the first minutes of cement hydration, the fraction of mobile water  
 344 molecules transiently present at solid interfaces  $N_S/N$  in presence of different nature and  
 345 quantity of cellulose ethers is a key result of this study that can be directly linked to the  
 346 relative amount of water retained on the pores surface.

347  
 348 We have applied the same NMRD method for starch ethers M1, M4 (Fig. 7) and found the  
 349 following results:  $d_0 = 11\text{ min} < d_{M4} = 19\text{ min} < d_{M1} = 22\text{ min}$  and  $R_0 = 30\text{ s}^{-1} <$



350  $R_{M4} = 33.6 \text{ s}^{-1} < R_{M1} = 35.2 \text{ s}^{-1}$  that reveal a much weaker microscopic water retention  
351 effect than the ones obtained with *CE* polymers.

352 Moreover, the effect of the substitution of *CE* on the water transiently present at the solid  
353 interfaces for HEMC C4 and HEC N7 molecules is shown on Fig. 8. These two polymers  
354 have been chosen to evidence the effect of hydrophobic methoxyl groups present on HEMC  
355 and absent on HEC. We check that the ASTM method cannot discriminate the important  
356 water retention (WR=98.8%) for the cements adjuvanted by these two polymers [31]. We  
357 remind that this discrimination is limited by the depression imposed by the method (50  
358 mmHg). To improve the sensibility of the ASTM method, one should increase largely such a  
359 depression. On the contrary, we show here that the NMRD data can indeed discriminate the  
360 observed value  $R_{CE}=39 \text{ s}^{-1}$  for the hydrophilic HEC N7 molecule and  $R_{CE}=37\text{s}^{-1}$  for the  
361 hydrophobic HEMC molecule, because NMR is very sensitive to the local environment of the  
362 proton spins. So the macroscopic ASTM measurement is not able to distinguish polymer's  
363 effect while NMRD is more sensitive to the local physical-chemistry at the solid interfaces.

364 Last, Fig. 9 shows the NMRD results for HPMC J1 with two different concentrations  
365 namely 0.1 and 0.4% giving 82.3 and 98.0% macroscopic water retention, respectively. As  
366 expected, the value of the plateau  $R_{CE}$  increases significantly with the concentration of  
367 admixture. Finally, on Fig. 10, the linear correlation ( $r^2 = 0.93$ ) of  $R_{CE}$  and water retention of  
368 mortar admixed with three different concentrations 0.1, 0.27 and 0.4% of HPMC J1 proves  
369 that our microscopic NMRD measurements on cement pastes could be correlated with the  
370 macroscopic water retention on mortars.

## 371 5. Conclusion

372 An original method based on two different applications of proton-water magnetic  
373 relaxation dispersion (NMRD) has been proposed to elucidate the effect of cellulose ethers  
374 (*CE*) on water retention of freshly-mixed white cement paste.

375 The first application of NMRD probes directly the proton-water surface dynamics from the  
376 magnetic field dependence of the nuclear spin-lattice relaxation rate. In spite of modifications  
377 of the solution's viscosity, we find that the cellulosic derivatives do not modify the surface  
378 diffusion coefficient of water that is about two orders of magnitude smaller than that of bulk  
379 water.

380 The second application of NMRD concerns the continuous measurements of the spin-  
381 lattice relaxation rates at a fixed and very low Larmor frequency. At the very early ages, this  
382 application probes continuously and for the first time, the relative population of water  
383 transiently present at the surface of the time-growing solid hydrate interfaces. Compared to  
384 neat white cement, the *CE* modify significantly the surface fraction of mobile water molecules  
385 transiently present initially at solid surfaces. Our results show that the larger the fraction, the  
386 better water-retention capacity of the hydrated cement or mortar samples at the proximity of a  
387 solid support. This quantity measured for all admixed cement pastes is thus relevant to  
388 explain the water retention mechanism. Furthermore, a linear correlation is found between the  
389 NMR surface fraction and the standard ASTM method used by the mortar industry to estimate  
390 the water retention capacity of admixed mortars. However for very strong water retention, it  
391 seems that the ASTM is not able to distinguish the polymer's effect while NMRD enables us  
392 to make the difference between two admixtures.

393

#### 394 **Acknowledgements**

395 The authors acknowledge all the industrial and academic CReM members  
396 (<http://cerem.cstb.fr>).

397

- 399 [1] S. Mansoutre, P. Colombet, H. Van Damme. *Water retention and granular rheological*  
400 *behavior of fresh C3S paste as a function of concentration.* Cem. Concr. Res., **29** (1999)  
401 1441-1453.
- 402 [2] A. Peschard, A. Govin, P. Grosseau, B. Guilhot, R. Guyonnet. *Effect of polysaccharides*  
403 *on the hydration of cement paste at early ages.* Cem. Concr. Res., **34** (2004) 2153–2158.
- 404 [3] J. Pourchez, A. Peschard, P. Grosseau, R. Guyonnet, B. Guilhot, F. Vallée. *HPMC and*  
405 *HEMC influence on cement hydration.* Cem. Concr. Res., **36** (2006) 1777-1780.
- 406 [4] J. Pourchez, B. Ruot, J. Debayle, E. Pourchez, P. Grosseau. *Some aspects of cellulose*  
407 *ethers influence on water transport and porous structure of cement-based materials.*  
408 Cem. Concr. Res., **40** (2010) 242-252.
- 409 [5] L. Patural, P. Marchal, A. Govin, P. Grosseau, B. Ruot, O. Devès. *Cellulose ethers*  
410 *influence on water retention and consistency in cement-based mortars.* Cem. Concr.  
411 Res., **41** (2011) 46-55.
- 412 [6] H. Kuhn, D. H. Waldeck, H.-D. Försterling. *Principles of Physical Chemistry.* Wiley-  
413 Interscience (2009).
- 414 [7] B. Penke, S. Kinsey, S. J. Gibbs, T. S. Moerland, B. R. Locke. *Proton Diffusion and T1*  
415 *Relaxation in Polyacrylamide Gels: A Unified Approach Using Volume Averaging.* J.  
416 Magn. Reson., **132** (1998) 240-258.
- 417 [8] N. Nestle, A. Kühn, K. Friedemann, C. Horch, F. Stallmach, G. Herth, *Water balance*  
418 *and pore structure development in cement materials in internal curing with modified*  
419 *superabsorbent polymer studied by NMR, Microporous and Mesoporous Materials* **125**  
420 *(2009) 51-57.*
- 421 [9] L. Patural, P. Porion, H. Van Damme, A. Govin, Ph. Grosseau, B. Ruot, O. Devès, A  
422 *pulsed field gradient and NMR imaging investigations of the water retention*

- 423 *mechanism by cellulose ethers in mortars*, Cem. Concr. Res., **40** (2010) 1378-1385.
- 424 [10] A. G. Redfield, W. Fite, H.E. Bleich, *Precision high speed current regulators for*  
425 *occasionally switched inductive loads*, Rev. Sci. Instrum., **39** (1968) 710-715.
- 426 [11] F. Noack, *Basic and novel aspects of NMR field-cycling spectroscopy*, Bull. Ampere,  
427 **175** (1994) 18-35.
- 428 [12] J.-P. Korb, L. Monteilhet, P.J. McDonald, J. Mitchell. *Microstructure and texture of*  
429 *hydrated cement-based materials: A proton field cycling relaxometry approach*. Cem.  
430 Concr. Res., **37** (2007) 295-302
- 431 [13] H.F.W. Taylor, *Cement Chemistry, 2<sup>nd</sup> edition*, Academic Press Thomas Telford (2007).
- 432 [14] F. Crössmann, W. Klaus. *Wasserlösliche Celluloseäther im Spiegel der*  
433 *Anwendungstechnik*. Collection of publication of a group of authors of Kalle, branch of  
434 Hoechst AG, Wiesbaden-Biebrich (1974).
- 435 [15] C. Clasen, W.-M. Kulicke. *Determination of viscoelastic and rheo-optical material*  
436 *functions of water-soluble cellulose derivatives*. Prog. Polym. Sci., **26** (2001) 1839-1919.
- 437 [16] B. Ruot, T. Goto, J. Pourchez. *Some aspects of cellulose ethers and latexes influence on*  
438 *the properties of cement-based materials - Examples of results obtained within the*  
439 *CEReM*. Proceedings of the VII SBTA (7<sup>o</sup> Symposio Brasileiro De Tecnologia Das  
440 Argamassas), (2007).
- 441 [17] EN 196-1. *Methods of testing cement — Part 1: Determination of strength*. (2006).
- 442 [18] Standard C1506-09. *Standard test Method fo Water Retention of Hydraulic Cement-*  
443 *Based Mortars and Plasters*. Am. Soc. Test. Mat. (2009).
- 444 [19] *Certifié CSTB Certified des enduits monocouches d'imperméabilisation – Modalités*  
445 *d'essais, DT 9 du 10 avril 2008*.
- 446 [20] F. Barberon, J.-P. Korb, D. Petit, V. Morin, E. Bermejo. *Probing the surface area of a*  
447 *cement-based material by nuclear magnetic relaxation dispersion*. Phys. Rev. Lett., **90**

- 448 (2003) 116103-116104.
- 449 [21] J.-P. Korb. *NMR and nuclear spin relaxation of cement and concrete materials*.  
450 *Curr. Opin. in Coll. Int. Sci.*, **14** (2009) 192-202.
- 451 [22] J.-P. Korb. *Microstructure and texture of cementitious porous materials*. *Magn. Res.*  
452 *Imag.*, **25** (2007) 466-469.
- 453 [23] I. Solomon, *Relaxation processes in a system of two spins*, *Phys. Rev.* **99**, (1955) 559-  
454 **565**.
- 455 [24] R.G. Bryant, D. A. Mendelson, C. Coolbaugh Lester, *The magnetic field dependence of*  
456 *proton spin relaxation in tissues*, *Magn. Reson. in Medicine* **21**, (1991) 117-126.
- 457 [25] K. R. Brownstein and C. E. Tarr, *Importance of classical diffusion in NMR studies of*  
458 *water in biological cells*, *Phys. Rev. A*, **19**, (1979) 2446-2453.
- 459 [26] J.-P. Korb, M. Whaley-Hodges, R. G. Bryant. *Translational diffusion of liquids at*  
460 *surfaces of microporous materials: Theoretical analysis of field-cycling magnetic*  
461 *relaxation measurements*. *Phys. Rev. E*, **56** (1997) 1934-1945.
- 462 [27] A. Abragam, *The principles of Nuclear Magnetism*, Ch 8, (Clarendon, Oxford, 1961).
- 463 [28] N. Bloembergen and L. O. Morgan, *Proton relaxation times in paramagnetic solutions;*  
464 *effects of electron spin relaxation*, *J. Chem. Phys.*, **34**, 842 (1961).
- 465 [29] A. Plassais, M.-P. Pomies, N. Lequeux, J.-P. Korb, D. Petit, F. Barberon,  
466 *Microstructure evolution of hydrated cement pastes*, *Phys. Rev. E*, **72** (2005) 041401-  
467 041408.
- 468 [30] J. J. Fripiat, M. Letellier, and P. Levitz, *Interaction of Water with Clay Surfaces*, *Phil.*  
469 *Trans. R. Soc. A*, **311** (1984) 287-299.
- 470 [31] L. Patural, PhD Thesis, ENSM (2011).

471 **Table 1.** Phase composition of the white cement.

Phases	C <sub>3</sub> S	C <sub>2</sub> S	C <sub>3</sub> A	C <sub>4</sub> AF	Sulfates
Phase composition (%)	68.8 ± 0.3	10.4 ± 0.7	10.5 ± 0.1	1.0 ± 0.1	7.5 ± 0.1

472 **Table 2.** Molecular parameters and water retention for cellulose ethers used in this work.

CE	$\overline{M}_w$ (kDa)	OCH <sub>3</sub> (%) <sup>a</sup>	DS	OC <sub>2</sub> H <sub>4</sub> OH (%) <sup>a</sup>	OC <sub>3</sub> H <sub>6</sub> OH (%) <sup>a</sup>	MS	Water retention (%)
HEMC C4	380	27.4	1.7	4.80	-	0.15	98.8
HPMC J1	225	28.2	1.8	-	2.98	0.10	96.8
HPMC J2	630	28.2	1.8	-	2.98	0.10	98.6
HPMC J3	910	28.2	1.8	-	2.98	0.10	98.9
HEC N7	2 900	-	-	56.0	-	2.5	98.8

473 <sup>a</sup> Informations provided by the manufacturer.

474 Mw=Cellulose ether weight-average molecular mass determined using size exclusion chromatography

475 DS= Number of substituted hydroxyl groups per anhydroglucose unit expressed as degree of substitution

476 MS=Molar ratio of alkoxy groups in the side chains to cellulose expressed as the average molecular substitution

477 OCH<sub>3</sub>= Methoxy group

478 OC<sub>2</sub>H<sub>4</sub>OH= Hydroxyethyl group

479 OC<sub>3</sub>H<sub>6</sub>=Hydroxypropyl group

480 **Table 3.** Molecular parameters and water retention for starch ethers (SE) used in this work.

SE	$\overline{M}_w$ (kDa)	Amylopectin / amylose ratio <sup>a</sup>	Degrees of polymerization <sup>a</sup>		Water retention (%)
			Amylose	Amylopectin	
SE M1	860	80 / 20	4 000	2 000 000	92.6
SE M4	830	80 / 20	4 000	2 000 000	66.2

481 <sup>a</sup> Informations provided by the manufacturer.

482

483

### Figure captions

484 **Fig. 1.** Structure of cellulose ethers (a): HPMC, (b): HEMC, (c): HEC. Substituent positions  
485 are arbitrary; they may differ slightly from one molecule to another.

486 **Fig. 2.** Experimental device to measure water retention with ASTM C1506-09 standard.

487 **Fig. 3.** Measured water  $^1\text{H}$  magnetic relaxation dispersion profiles for hydrated white cement  
488 paste ( $w/c=0.4$ ) as a function of the proton Larmor frequency. The experiments have been  
489 realized in the early hydration period (0-45 min, filled circles) and on a larger hydration time  
490 (up to few hours, filled squares) for neat (without *CE*) cement (**a**) and cement admixed with  
491 HPMC J3 (**b**). The continuous lines are the best fits obtained with Eqs. (2) and (3).

492 **Fig. 4.** Measured water  $^1\text{H}$  spin-lattice relaxation rates of hydrated white cement pastes  
493 ( $w/c=0.4$ ) as a function of the proton Larmor frequency. (a) Effect of three cellulose ethers  
494 (HPMC J1, J2, J3). The J3 data sets are the same as those in Fig. 3. (b) Effect of two starch  
495 ethers (M1 and M4). In both cases, we have reported the results obtained with the neat white  
496 cement paste. The continuous lines are the best fits obtained with Eqs. (2) and (3).

497 **Fig. 5.** Water  $^1\text{H}$  spin-lattice relaxation rates of hydrated cement pastes ( $w/c=0.4$ ) as a  
498 function of hydrating time measured at a Larmor frequency of 10 kHz. Effect of three  
499 cellulose ethers (HPMC, J1, J2, J3). The inset represents a zoom on the frequency range of the  
500 plateau.

501 **Fig. 6.** Correlation between the delays obtained by the NMRD and isotherm calorimetry.  
502

503 **Fig. 7.** Water  $^1\text{H}$  spin-lattice relaxation rates of hydrated cement pastes ( $w/c=0.4$ ) as a function  
504 of hydrating time measured at a Larmor frequency of 10 kHz. Effect of three cellulose ethers

505 (Neat, starch CE: M1, M4). The inset represents a zoom on the frequency range of the ,  
506 plateau.

507 **Fig. 8.** Comparison of the water  $^1\text{H}$  spin-lattice relaxation rates of hydrated cement pastes  
508 ( $w/c=0.4$ ) as a function of hydrating time measured at a Larmor frequency of 10 kHz. Effect  
509 of different cellulose ethers (Neat, HEC N7, HEMC C).

510 **Fig. 9.** Comparison of the water  $^1\text{H}$  spin-lattice relaxation rates of hydrated cement pastes  
511 ( $w/c=0.4$ ) as a function of hydrating time measured at a Larmor frequency of 10 kHz. Effect  
512 of the *CE* concentration of HPMC.

513 **Fig. 10.** Correlation between the water retention evidenced from the macroscopic  
514 measurement described in Fig. 2 (ASTM C1506-09 standard) and the NMRD method. The  
515 different concentrations of HPMC J1 are indicated.

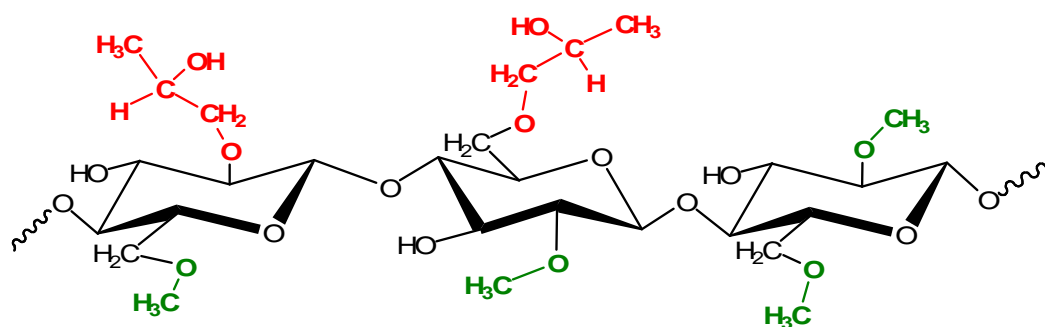
516



517

518

(a)

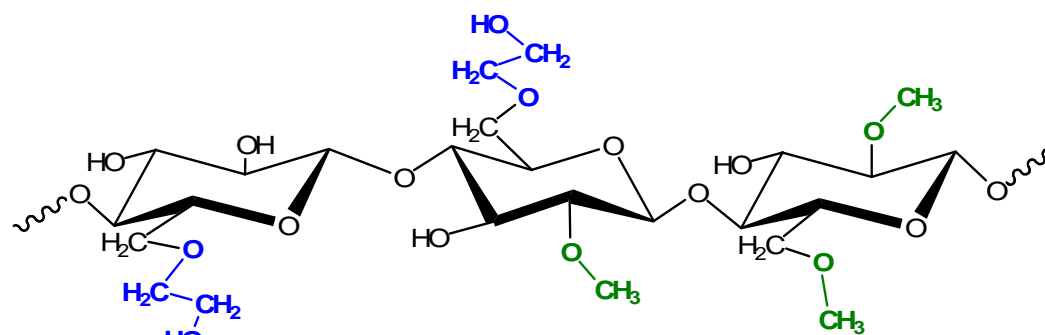


519

520

521

(b)

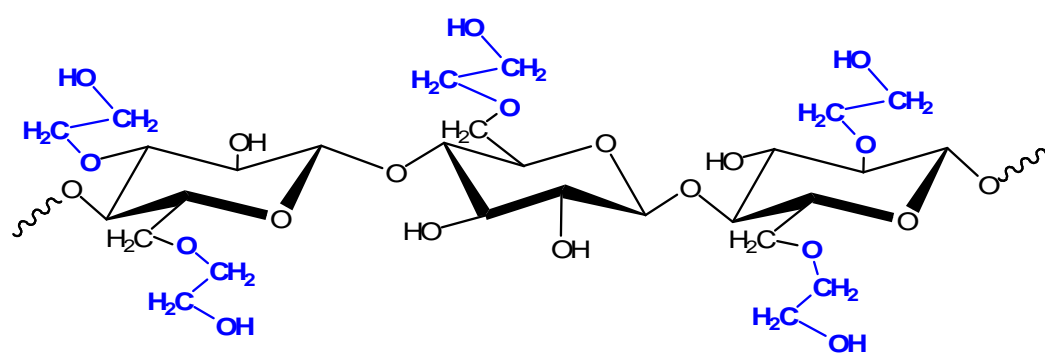


522

523

524

(c)

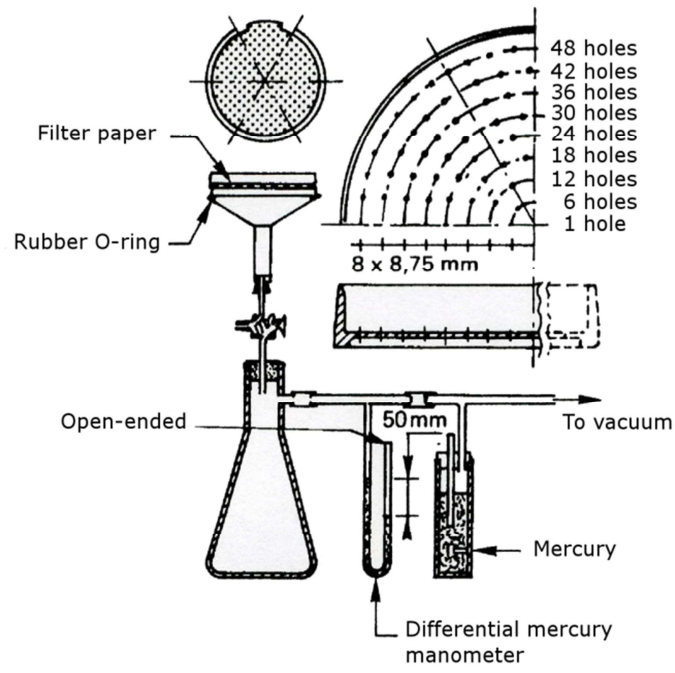


525

526

Fig. 1

527



528

529

530

Fig.2

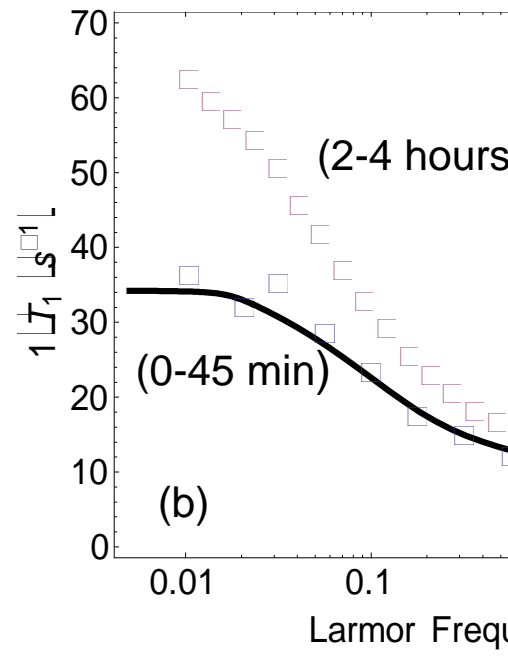
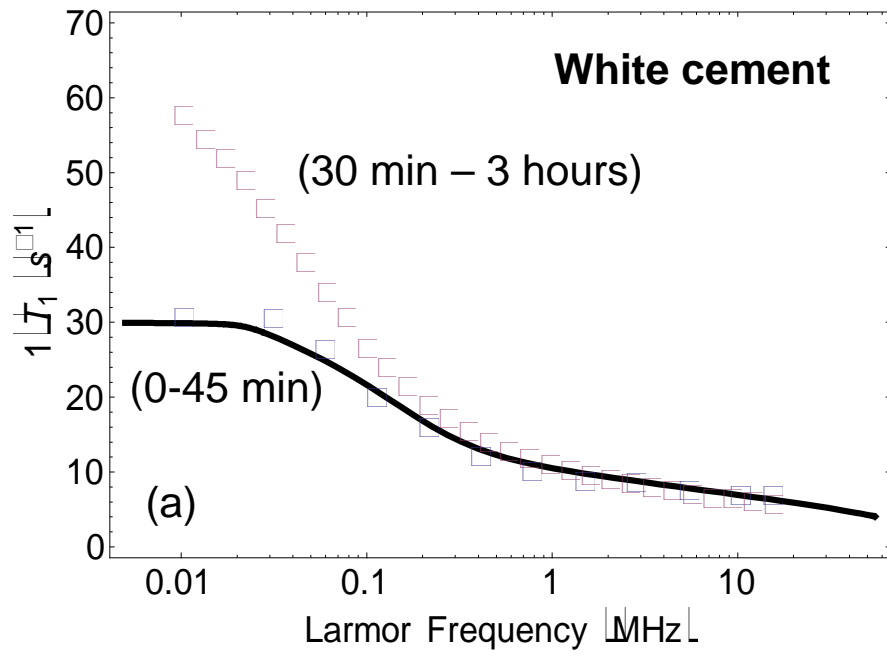


Fig. 3

531  
532

533

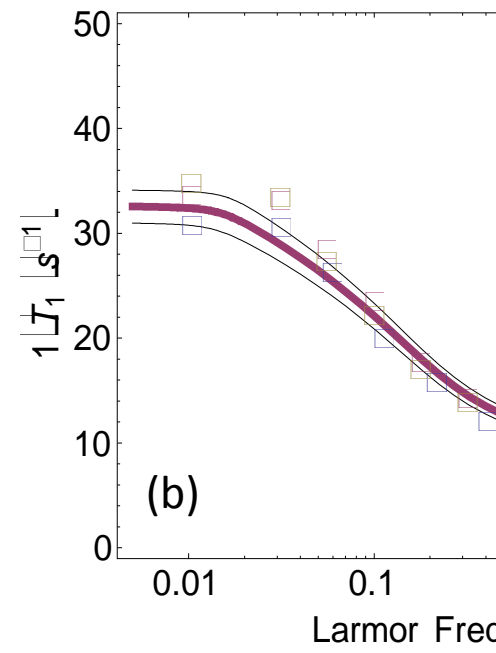
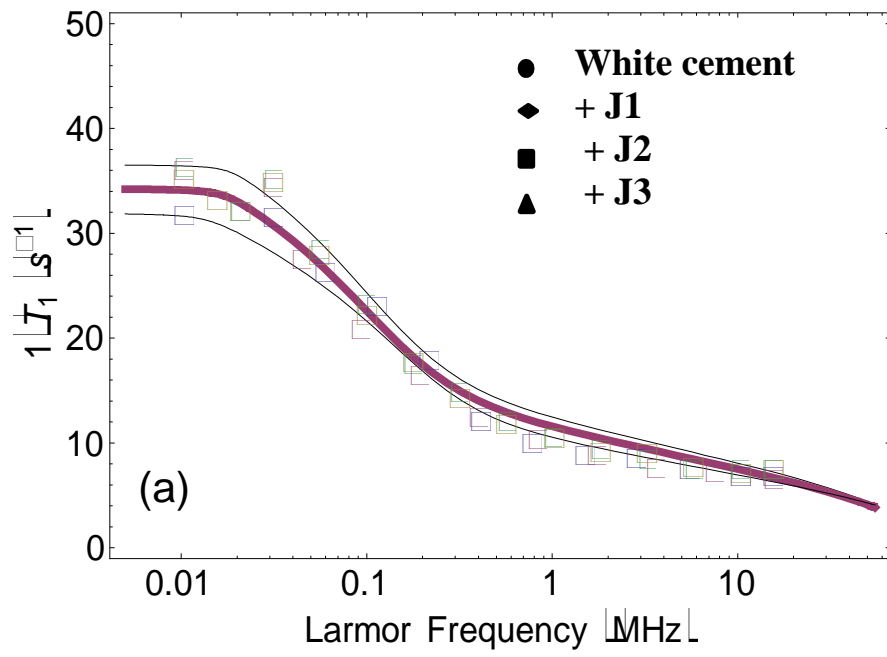


Fig.4

535  
536  
537  
538  
539  
540

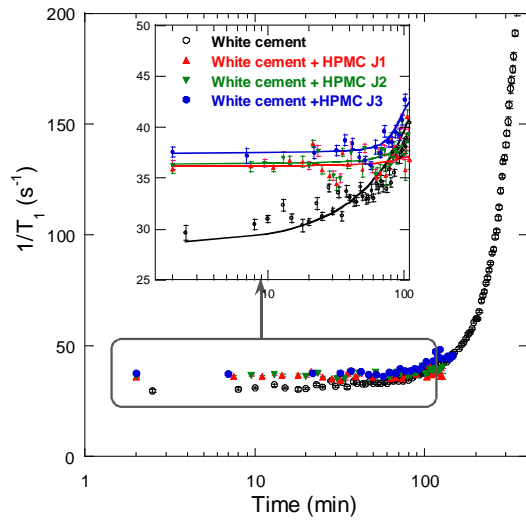
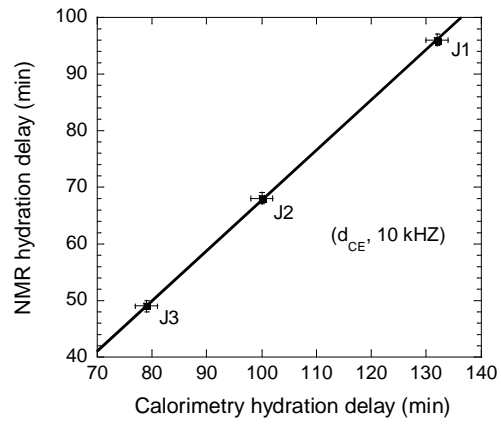


Fig. 5

541  
542  
543

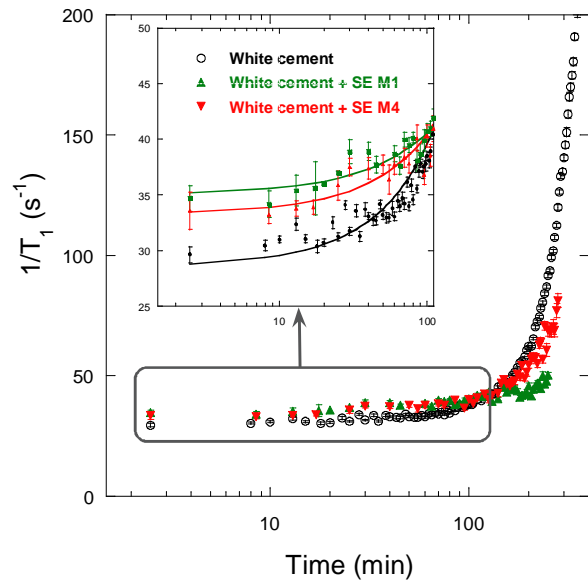


544

545

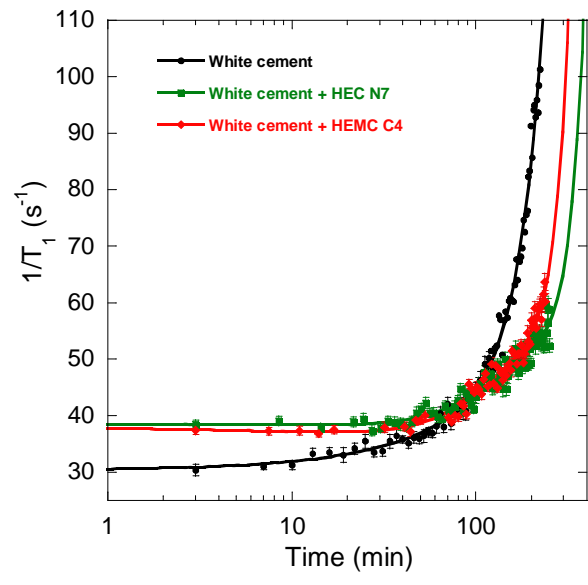
546

Fig. 6



547  
 548  
 549  
 550

Fig. 7



551  
552  
553  
554

Fig. 8



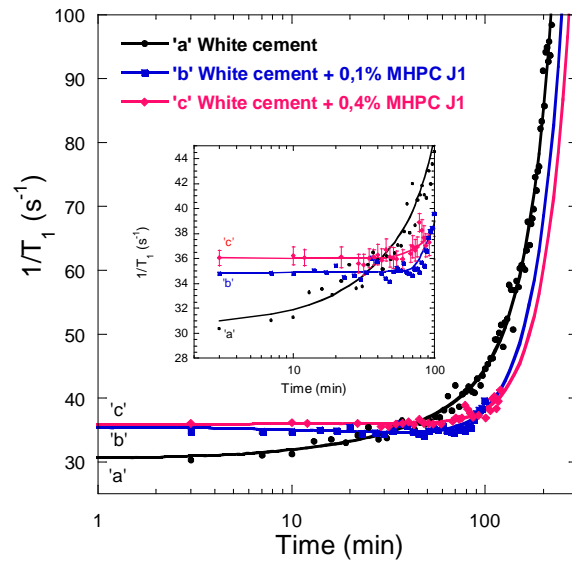
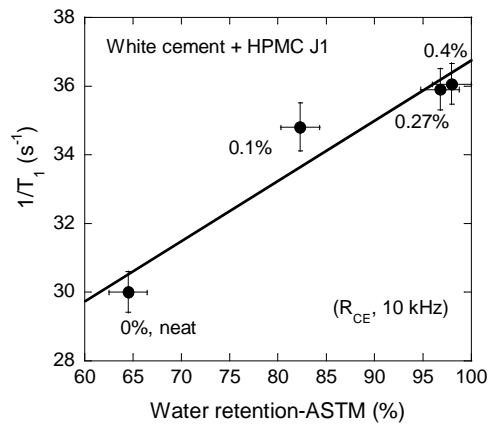


Fig. 9

555  
556  
557



558

559

560

Fig. 10